

Symmetry breaking in binary chain with nonlinear sites

Dmitrii N. Maksimov and Almas F. Sadreev
Institute of Physics, 660036, Krasnoyarsk, Russia
(Dated: March 21, 2018)

We consider a system of two or four nonlinear sites coupled with binary chain waveguides. When a monochromatic wave is injected into the first (symmetric) propagation channel the presence of cubic nonlinearity can lead to symmetry breaking giving rise to emission of antisymmetric wave into the second (antisymmetric) propagation channel of the waveguides. We found that in the case of nonlinear plaquette there is a domain in the parameter space where neither symmetry preserving nor symmetry breaking stable stationary solutions exist. As a result injection of a monochromatic symmetric wave gives rise to emission of nonsymmetric satellite waves with energies different from the energy of the incident wave. Thus, the response exhibits nonmonochromatic behavior.

PACS numbers: 03.75.-b,05.45-a,42.65.Ky,42.65.Pc,42

I. INTRODUCTION

To the best of our knowledge symmetry breaking (SB) in the nonlinear systems was first predicted by Akhmediev who considered a composite structure of a single linear layer between two symmetrically positioned nonlinear layers [1]. One could easily see that if the wave length is larger than the thickness of the nonlinear layers then Akhmediev's model could be reduced to a dimer governed by the nonlinear Schrödinger equation. Independently the SB was discovered for the discrete nonlinear Schrödinger equation with a finite number of coupled sites (nonlinear dimer, trimer, *etc*) [2–8]. For example, in the case of the nonlinear Schrödinger dimer Eilbeck *et al* found two different families of stationary solutions [2]. The first family is symmetric (antisymmetric) ($|\phi_1| = |\phi_2|$) while the second is nonsymmetric ($|\phi_1| \neq |\phi_2|$). This consideration was later extended to a nonlinear dimer embedded into an infinite linear chain [9] with the same scenario for the SB. Multiple bifurcations to the symmetry breaking solutions were demonstrated by Wang *et al* [10] for the nonlinear Schrödinger equation with a square four-well potential. Remarkably, the above system can also support a stable state with a nodal point, i.e., quantum vortex [11]. In the framework of the nonlinear Schrödinger equation one can achieve bifurcation to the states with broken symmetry varying the chemical potential which is equivalent to the variation of the population of the nonlinear sites or, analogously, of the constant in the nonlinear term of the Hamiltonian. In practice, however, one would resort to the optical counterparts of the quantum nonlinear systems where the variation of the amplitude of the injected wave affects the strength of Kerr nonlinearity (see Refs. [12–22] for optical examples of the SB).

In the present paper we consider a nonlinear dimer and a square four-site nonlinear plaquette coupled with two channel waveguides in the form of binary tight-binding chains. The latter system is analogous to that recently considered in Ref. [23] where the plaquette however was set up without mirror symmetry with respect to the centerline of the waveguide. Due to nonlinearity of the plaquette the system can spontaneously bifurcate between diode-antidiode and bidirectional transmission regimes. In our case, we will show that when a monochromatic wave is injected into the first (symmetric) propagation channel the presence of the cubic nonlinearity can lead to symmetry breaking giving rise to emission of antisymmetric wave into the second (antisymmetric) propagation channel of the waveguides.

This result raises an important question about the effect of a probing wave on the SB. To allow for symmetry breaking the architecture of the open system should support some symmetries of its closed counterpart. When the growth of the injected power can result in bifurcations into the states violating the symmetry of the probing wave by the amplitude of the scattering function [12–14, 17, 18, 20, 21, 24] or by its phase [25].

The second important question is whether the solutions in the linear waveguides could be stationary monochromatic plane waves, reflected $\psi(n, t) = R \exp(-ikn - iE(k)t)$ and transmitted $\psi(n, t) = T \exp(ikn - iE(k)t)$, where R and T are the reflection and transmission amplitudes. If the answer is positive then we can apply the Feshbach projection technique [26–30] and implement the formalism of non-Hermitian effective Hamiltonian (now nonlinear) which acts on the nonlinear sites only thus truncating the Hilbert space to the scattering region [21, 30]. When the radiation shifts of the energy levels are neglected that formalism reduces to the well known coupled mode theory (CMT) equations [31–34]. In the present paper we will show that there are domains in the parameter space where there are no stable stationary solutions. We will demonstrate numerically that a plane wave incident onto a nonlinear object gives rise to emission of multiple satellite waves with energies (frequencies) different from the energy (frequency) of the probing wave.

II. STRUCTURE LAY-OUT AND BASIC EQUATIONS

We consider two tight-binding structures shown in Fig. 1, nonlinear dimer (a) and nonlinear four-site square plaquette (b) coupled with linear binary chains. Each chain, left and right, supports two continua of plane waves

$$\psi_1^{(\pm)}(n, t) = \frac{1}{\sqrt{2|\sin k_1|}} \begin{pmatrix} 1 \\ 1 \end{pmatrix} \exp(\pm ik_1 n - iE(k_1)t), \quad \psi_2^{(\pm)}(n, t) = \frac{1}{\sqrt{2|\sin k_2|}} \begin{pmatrix} 1 \\ -1 \end{pmatrix} \exp(\pm ik_2 n - iE(k_2)t) \quad (1)$$

where indices $p = 1, 2$ enumerate continua or channels with the propagation bands given by

$$E(k_p) = -2 \cos k_p \mp 1, \quad -\pi \leq k_p \leq \pi. \quad (2)$$

In order to control the resonant transmission we adjust the hopping matrix element between the nonlinear sites and waveguides $\epsilon < 1$ [30] shown in Fig. 1 by dash lines. The coupling between nonlinear sites (shown in Fig. 1 by dash-dot line) is controlled by constant γ .

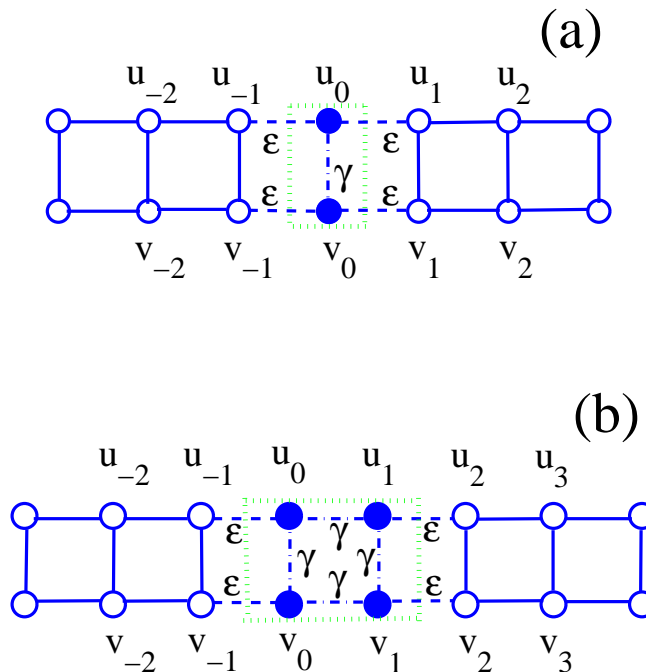


FIG. 1: (a) Two-channel waveguide in form of binary tight-binding chain which holds a nonlinear dimer (shown by filled circles). (b) The same as in subplot (a) but with four nonlinear sites (four-site plaquette). Green dotted box is placed around the nonlinear scattering region.

In the case of the nonlinear dimer the Schrödinger equation takes the following form

$$\begin{aligned} i\dot{u}_n &= -J_n u_{n+1} - J_{n-1} u_{n-1} - K_n v_n + \lambda \delta_{n,0} |u_n|^2 u_n, \\ i\dot{v}_n &= -J_n v_{n+1} - J_{n-1} v_{n-1} - K_n u_n + \lambda \delta_{n,0} |v_n|^2 v_n, \end{aligned} \quad (3)$$

where $J_n = 1 + (\epsilon - 1)(\delta_{n,-1} + \delta_{n,0})$, $K_n = 1 + (\gamma - 1)\delta_{n,0}$. In the case of nonlinear square plaquette the Schrödinger equation could be written down essentially in the same way.

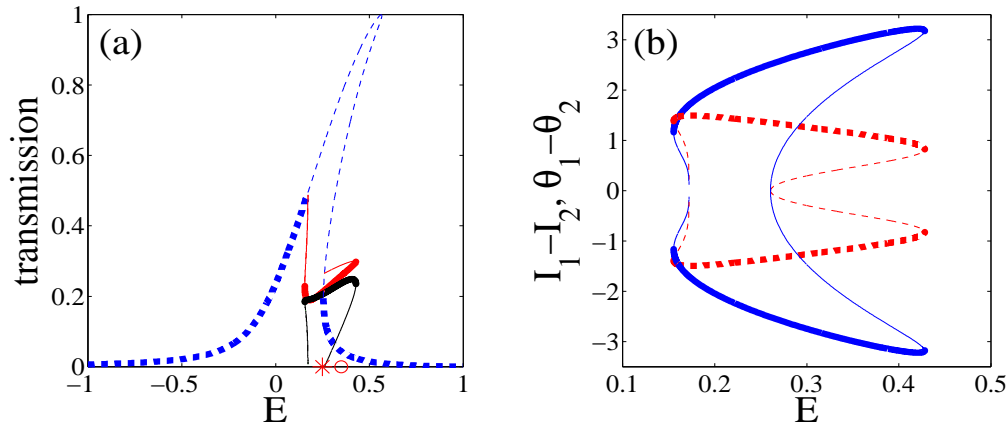


FIG. 2: (Color online) Response of nonlinear dimer to symmetric probing wave. (a) Transmission probability $|T_{11}|^2$ for symmetry preserving solution - blue dash line, $|T_{11}|^2$ for SB solutions - solid red line, $|T_{12}|^2$ for SB solutions - solid black. (b) Phase difference $\theta_2 - \theta_1$ for the pairs of SB solutions - dashed red line; intensity difference $I_1 - I_2$ - solid blue line. Thicker lines mark stable solutions. The parameters: $\epsilon = 0.2$, $A_0 = 1$, $\lambda = 0.025$, $\gamma = 0$.

III. NONLINEAR DIMER

First, let us follow Refs.[35–41] and search for the solution of the Schrödinger equation (3) in the form of a stationary wave

$$u_n(t) = u_n e^{-iEt}, v_n(t) = v_n e^{-iEt} \quad (4)$$

where the discrete space variable n and the time t are separated. The absence of nonlinearity in the waveguides drastically simplifies analysis of Eq. (3). Assuming that a symmetric/antisymmetric wave is incident from the left we can write the solutions in the left $\psi_L(n, t)$ and right $\psi_R(n, t)$ waveguides as:

$$\begin{aligned} \psi_L(n, t) &= A_0 \psi_p^{(+)}(n, t) + R_{p,1} \psi_1^{(-)}(n, t) + R_{p,2} \psi_2^{(-)}(n, t), \\ \psi_R(n, t) &= T_{p,1} \psi_1^{(+)}(n, t) + T_{p,2} \psi_2^{(+)}(n, t), \end{aligned} \quad (5)$$

where parameter A_0 is introduced to tune the intensity of the probing wave. Notice that Eq. (5) implicitly defines reflection and transmission amplitudes $R_{p,p'}$ and $T_{p,p'}$ with the first subscript p indexing the channels and respectively the symmetry of the incident wave. One can now match the solutions Eq. (5) to the equations for the nonlinear sites to obtain a set of nonlinear equations for on-site and reflection/transmission amplitudes. Computationally, however, it is more convenient to use the approach of the non-hermitian Hamiltonian [28, 30] in which the number of unknown variables equals to the number of nonlinear sites. Following Ref. [21] we write the equation for the amplitudes on the nonlinear sites

$$(E - H_{eff})|\psi\rangle = A_0 \epsilon |in\rangle \quad (6)$$

where

$$H_{eff} = H_0 - \sum_C V_C^\dagger \frac{1}{E + i0 - H_C} V_C = \begin{pmatrix} -\epsilon^2(e^{ik_1} + e^{ik_2}) + \lambda|u_0|^2 & -\gamma - \epsilon^2(e^{ik_1} - e^{ik_2}) \\ -\gamma - \epsilon^2(e^{ik_1} - e^{ik_2}) & \epsilon^2(e^{ik_1} + e^{ik_2}) + \lambda|v_0|^2 \end{pmatrix}. \quad (7)$$

Here vector $|\psi\rangle = (u_0, v_0)$ is the state vector of the dimer, H_0 is the nonlinear Hamiltonian of the dimer decoupled from the waveguides, V_C is the coupling operator [30] between the nonlinear sites and the left and right waveguides $C = L, R$ with the Hamiltonian H_C , and $|in\rangle = (1, \pm 1)$ is the source term for symmetric/antisymmetric incident waves correspondingly. One can easily see that in the limit $\epsilon \rightarrow 0$ the dimer is decoupled from the waveguides and Eq. (6) limits to the standard nonlinear Schrödinger equation of the closed nonlinear dimer. After Eq. (6) is solved one easily obtains transmission/reflection amplitudes from Eq. (3).

In Fig. 2 we present the response of the nonlinear dimer to a symmetric probing wave both in form of transmission probabilities $|T_{11}(E)|^2$, $|T_{12}(E)|^2$ Fig. 2(a), and phase $\theta_2 - \theta_1$ and intensity $I_1 - I_2$ differences Fig. 2(b). On-site

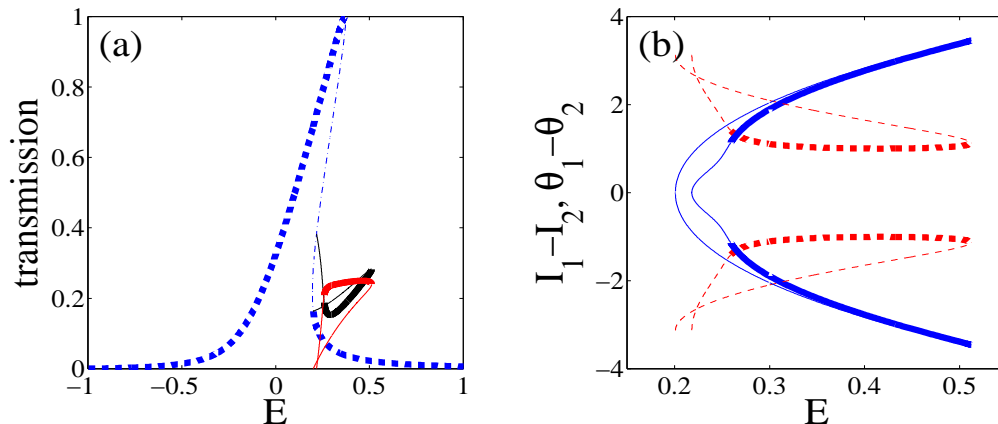


FIG. 3: (Color online) Response of nonlinear dimer to antisymmetric probing wave. (a) Transmission probability $|T_{22}|^2$ for the symmetry preserving solution - blue dash line; $|T_{22}|^2$ for SB solutions - solid red line, $|T_{21}|^2$ SB solutions - solid black line. (b) Phase difference $\theta_2 - \theta_1$ for the pairs of SB solutions - dashed red lines, intensity difference $I_1 - I_2$ - solid blue lines. Thicker lines mark stable solutions. The parameters: $\epsilon = 0.2$, $A_0 = 1$, $\lambda = 0.03$, $\gamma = 0$.

phases and intensities are defined through $u_0 = \sqrt{I_1}e^{i\theta_1}$, $v_0 = \sqrt{I_2}e^{i\theta_2}$. There are two principally different families of solutions similar to those obtained in Ref. [21]. The symmetry preserving family inherits the features of the linear case in which a symmetric probing wave excites only symmetric mode $\phi_s = \frac{1}{\sqrt{2}}(1, 1)$ with eigenvalue $E_s = -\gamma$. In fact, we see a typical example of nonlinear transmission through a resonant state. The transmission probability $|T_{11}(E)|^2$ for the symmetry preserving family of solutions with $I_1 = I_2$, $\theta_1 = \theta_2$ are shown in Fig. 2 (a) by blue dashed lines. The energy behavior of the transmission is very similar to the case of a linear waveguide coupled with one nonlinear in-channel site [35, 36, 42]. However, one can see that the peak of the resonant transmission is now unstable which is a key to mode conversion as it will be shown below. The stability of the solutions was examined by standard methods based on small perturbations technique (see, for example, Refs. [43, 44]).

The SB occurs due to excitation of the second (antisymmetric) mode of the dimer $\phi_a = \frac{1}{\sqrt{2}}(1, -1)$ with eigenvalue $E_a = \gamma$. The phase and intensity differences for the SB solutions are shown in Fig. 2(b). One can see that the symmetry is broken simultaneously by both intensity $I_1 \neq I_2$ and phase $\theta_1 \neq \theta_2$ of the wave function. This scenario of SB differs from the case of the closed dimer [2, 3, 5] or the dimer opened to a single chain (off-channel architecture) [21] where the symmetry was broken either by the intensities or by the phases of the on-site amplitudes.

In Fig. 3 we show the case when the antisymmetric wave is injected to the system. Although the energy behavior of the on-site intensities, on-site phases, and the transmission probabilities to the first and second channels $|T_{21}|^2$, $|T_{22}|^2$ is similar to the case of symmetric probing wave, the stability pattern of the symmetry preserving solution is now typical for the nonlinear transmission through a single nonlinear site Ref. [42]. Finally, following Ref. [45] we present the plots output vs. input, i.e., transmission probabilities $|T_{p,p'}|^2$ vs. A_0^2 for both symmetric and antisymmetric probing waves. In Fig. 4 one can see that the input-output curves for the symmetry preserving family of solutions have typical bifurcation behavior while the symmetry breaking family exists only within a bounded domain of the input.

As was mentioned above the SB phenomenon results in the mode conversion, i.e., emission of scattered waves into a different channel. Let us consider time evolution of the wave front given by

$$|\psi_{in}(n)\rangle = f(n)\psi_1^{(+)}(n, 0), \quad (8)$$

where

$$f(n) = \begin{cases} 1 & \text{if } n \leq -100; \\ e^{-(n+100)^2/250} & \text{if } n > -100, \end{cases} \quad (9)$$

is an auxiliary function that provides a smooth increase of incident plane wave amplitude. As the wave front propagates to the right the input signal converges to $\psi_1^{(+)}(n, t)$ so one could expect that in course of time the system would stabilize in one of the solutions shown in Fig. 2. In order to perform numerical computations we directly applied both standard fourth order Runge-Kutta method and the Besse-Crank-Nicolson relaxation scheme [46] to Eq. (3) with both techniques yielding the same result (Crank-Nicolson approach being slightly advantageous in terms of computational time). The

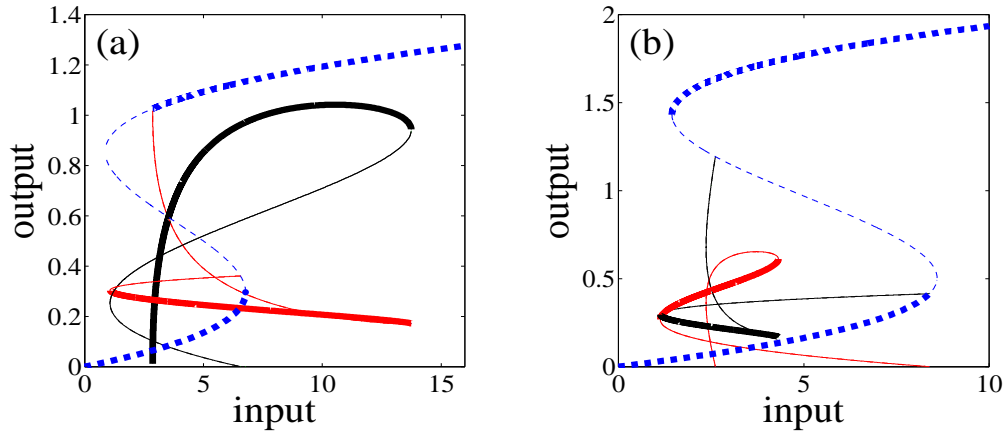


FIG. 4: (Color online) Input A_0^2 vs. outputs $|T_{p,p'}|^2$ for nonlinear dimer. (a) Symmetric probing wave $\langle in \rangle = (1, 1)$, $|T_{11}|^2$ - blue dash line symmetry preserving solutions, $|T_{11}|^2$ SB solutions - solid red line, $|T_{12}|^2$ SB solutions - solid black line. (b) Antisymmetric probing wave $\langle in \rangle = (1, -1)$, $|T_{22}|^2$ - blue dash line symmetry preserving solutions, $|T_{22}|^2$ SB solutions - solid red line, $|T_{21}|^2$ SB solutions - solid black. The parameters: $\epsilon = 0.2$, $E = 0.45$, $\lambda = 0.025$, $\gamma = 0$.

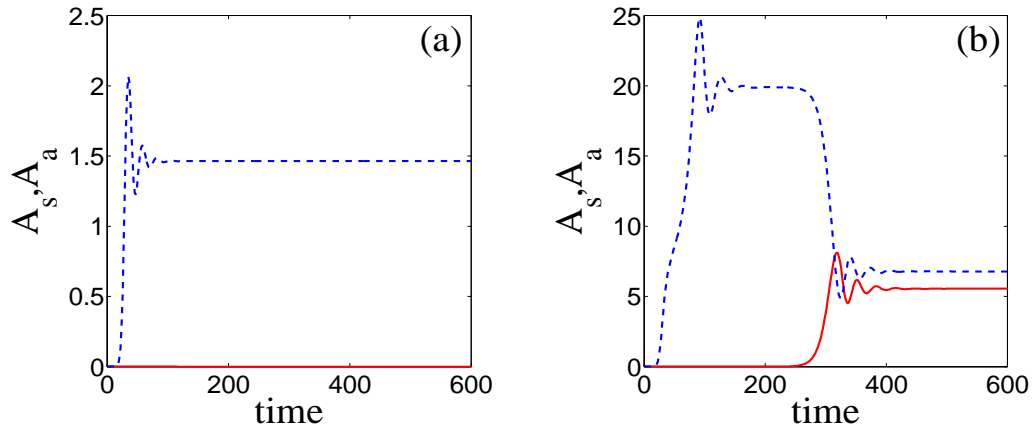


FIG. 5: (Color online) Time evolution of populations A_s - dashed blue line, A_a - solid red line. $\epsilon = 0.2$, $A_0 = 1$, $\lambda = 0.025$, $\gamma = 0$. (a) Stable symmetry preserving solution $E = 0.35$ (red circle in Fig. 2(a)). (b) Unstable symmetry preserving solution $E = 0.25$ (red star in Fig. 1(a)). The parameters: $\epsilon = 0.2$, $A_0 = 1$, $\lambda = 0.025$, $\gamma = 0$

absorbing boundary conditions were enforced at far ends of the waveguides according to Ref. [47] to truncate the problem to a finite domain.

Let us first choose the energy in the domain where the symmetry preserving solution is stable, for example $E = 0.35$ (shown in Fig. 2(a) by red circle). To detect the SB we use the populations A_s and A_a of the symmetric ϕ_s and antisymmetric ϕ_a modes correspondingly. Fig. 5(a) shows that although stable SB solutions exist at $E = 0.35$ the response to the probing signal Eq. (8) contains only symmetric contribution and after several oscillations converges to the stationary transmission. On the other hand, if one chooses the energy of the incident wave from the domain where the symmetry preserving solutions are unstable $E = 0.25$ (shown in Fig. 2(a) by red star), the system first stabilizes in an unstable symmetry preserving solution but then, due to accumulation of numerical round-off error, it is forced to leave the unstable equilibrium and occupy one of the stable states with broken symmetry Fig. 3(a). Thus, the round-off error induces the SB playing the role of noise in a real experiment. It is important to notice that the results in Fig. 5 agree with the data obtained with the use of the effective non-Hermitian Hamiltonian Eq. (6).

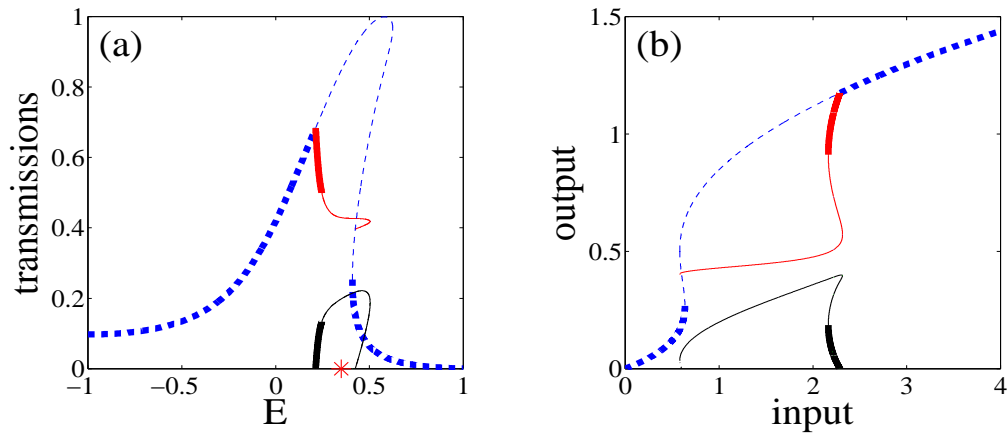


FIG. 6: (Color online) Response of nonlinear plaquette to symmetric probing wave $\epsilon = 0.4, \gamma = 1, \lambda = 0.09$, transmission probability $|T_{11}|^2$ for symmetry preserving solutions - dashed blue line, $|T_{11}|^2$ SB solutions - solid red line, $|T_{12}|^2$ SB solutions - solid black. (a) Transmissions vs. energy, $A = 1$. (b) Transmissions vs. A^2 , $E = 0.35$. Thicker lines mark stable solutions. In both cases one can see windows where neither symmetry preserving nor symmetry breaking stable solutions exist.

IV. FOUR-SITE NONLINEAR PLAQUETTE

In the previous section we demonstrated how the phenomenon of SB occurs in the nonlinear dimer due to resonant excitation of both symmetric and antisymmetric modes ϕ_s, ϕ_a . Notice that a necessary condition for the SB is that both modes be near degenerate to be excited at the same energy. This forced us to choose the inner coupling constant $\gamma = 0$. In fact, our numerical tests show that the SB will quickly vanish as γ increased. In that sense the set-up of four-site plaquette seems more feasible because now the closed system supports two degenerate modes of different symmetries at any value of γ , namely $\langle \chi_s | = \frac{1}{2}(1, 1, -1, -1)$ and $\langle \chi_a | = \frac{1}{2}(1, -1, 1, -1)$. The corresponding degenerate eigenvalue is $E_{s,a} = 0$.

In the case of the four-site plaquette the effective Hamiltonian takes the following form [28, 30]

$$H_{eff} = \begin{pmatrix} -\epsilon^2(e^{ik_1} + e^{ik_2})/2 + \lambda|u_0|^2 & -\gamma - \epsilon^2(e^{ik_1} - e^{ik_2})/2 & -\gamma & 0 \\ -\gamma - \epsilon^2(e^{ik_1} - e^{ik_2})/2 & -\epsilon^2(e^{ik_1} + e^{ik_2})/2 + \lambda|v_0|^2 & 0 & -\gamma \\ -\gamma & 0 & -\epsilon^2(e^{ik_1} + e^{ik_2})/2 + \lambda|u_1|^2 & -\gamma - \epsilon^2(e^{ik_1} - e^{ik_2})/2 \\ 0 & -\gamma & -\gamma - \epsilon^2(e^{ik_1} - e^{ik_2})/2 & -\epsilon^2(e^{ik_1} + e^{ik_2})/2 + \lambda|v_1|^2 \end{pmatrix}. \quad (10)$$

Eq. (6) should now be solved for the state vector of the plaquette $|\psi\rangle = (u_0, v_0, u_1, v_1)$ (see Fig. 1(b)) with the source term $\langle in | = (1, \pm 1, 0, 0)$. The results of numerical solution are presented in Fig. 6.

Although the result is similar to the case of nonlinear dimer (Figs. 2 and 3) there is one important difference. Namely, there is now a domain in the parameter space where *all* stationary solutions are unstable as shown in Figs. 6. Respectively, the solution of the transmission problem in such system can be described neither by transmission and reflection amplitudes Eqs. (5) nor by the Feshbach projection method, i.e. by the effective non-Hermitian Hamiltonian Eq. (6). The problem of plane wave scattering from the nonlinear plaquette can only be solved through numerical simulation of the time-dependent equation.

To perform numerical tests we repeated the wave-front simulations explained in the previous section. Fig. 7 shows the time evolution of populations A_s, A_a of symmetric and antisymmetric resonant modes $|\chi_s\rangle, |\chi_a\rangle$. At $t = 0$ a symmetric wave front (8) is sent from the left waveguide towards the plaquette with its energy and amplitude within the domain of unstable stationary solutions $E = 0.4$ (shown by red star in Fig 6(a)). First when $t \in [150, 350]$ only symmetric state of the plaquette is excited; $A_a = 0$. However, the symmetry preserving solution is unstable. That causes transition to the symmetry breaking solution $A_a > 0$ at $t \approx 400$. As a result the plaquette emits stationary plane waves of both symmetries with the same energy as the probing wave when $t \in [450, 650]$. Since this solution is also unstable the system transits to another regime at $t \approx 700$. It is clearly seen in Fig. 7 that in this regime the solution is also symmetry breaking, however, what is more interesting, it is *non-stationary*. The Fourier power spectrum $F(E)$ Fig. 8 of the amplitude u_3 (see Fig. 1) for $t \geq 800$ clearly shows the presence of three peaks, the central peak with energy $E = 0.4$ and two satellites with energies $E_1 = -1.71, E_2 = 2.51$.

With the growth of the nonlinearity constant λ which is equivalent to growth of the amplitude of the injected wave the dynamical properties of the nonlinear plaquette change drastically. Fig. 9(a) shows the transmission probabilities

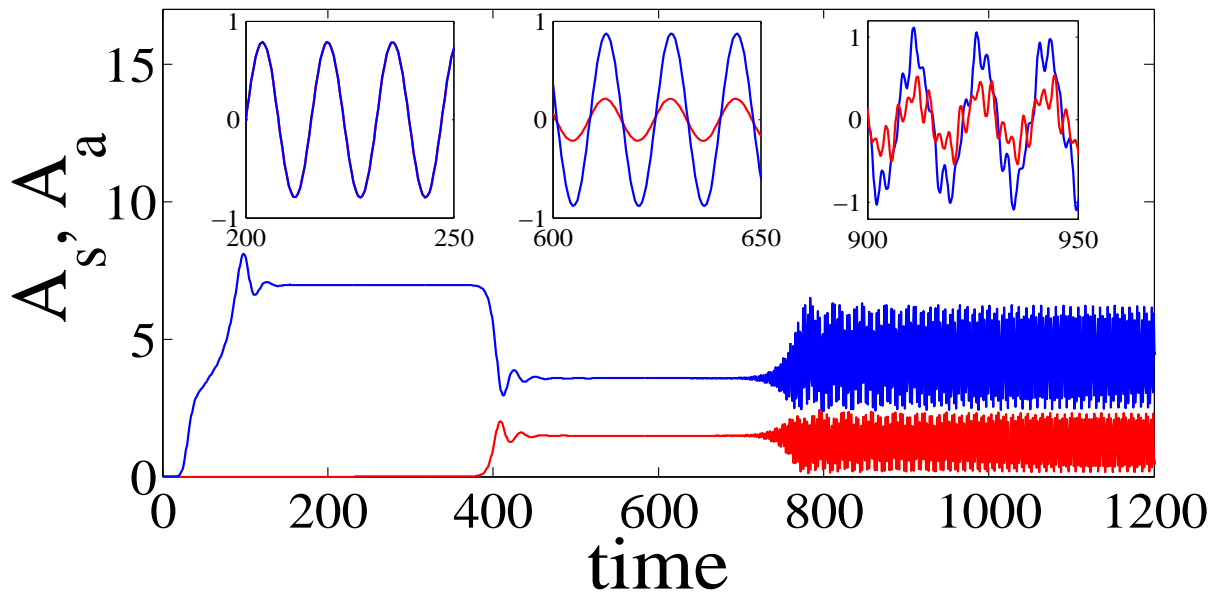


FIG. 7: (Color online) Time evolution of populations of symmetric B_s (blue line), and antisymmetric B_a (red line) resonant modes, $\epsilon = 0.4$, $\gamma = 1$, $\lambda = 0.09E = 0.4$. The insets show the real parts of amplitudes u_3 (blue line), and v_3 (red line) vs. time t in the corresponding regimes. One can clearly see that in course of time the system evolves to a non-stationary solution.

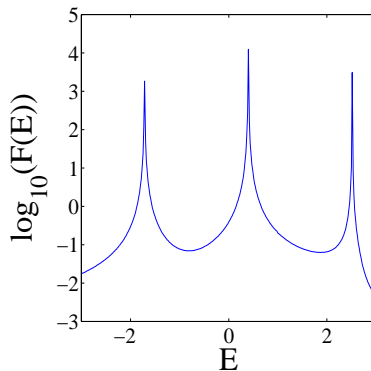


FIG. 8: (Color online) Logarithmic plot of Fourier power spectrum of output amplitude u_3 in the non-stationary regime Fig. 7.

vs. the incident energy. One can see that compared against Fig. 6 the transmission peak is now shifted towards the edge of the propagation band. When the energy of the incident wave belongs to the instability window of the symmetry preserving solution $E = 0.5$ (red star in Fig. 9(a)) the system rapidly evolves to non-stationary symmetry breaking regime. The time-Fourier power spectrum with several equidistant satellite peaks is shown in Fig 9(b). It should be noticed that although there now is a pair of stable symmetry breaking solutions at $E = 0.5$ the system nevertheless does not access them but immediately transits to the non-stationary regime. That phenomenon of satellite peak generation obviously differs from the second harmonic generation where the waves of twice the energy (frequency) would be emitted [48].

V. SUMMARY AND DISCUSSION

In this paper we considered the simplest nonlinear open systems whose closed analogues allow for symmetry breaking, namely, dimer and four-site square plaquette [2–8]. The term "open" means that linear waveguides are now attached to the nonlinear objects. The waveguides are chosen in the form of tight-binding double chains. As shown in Fig. 1 this architecture preserves the mirror symmetry with respect to the center-line of the waveguides. Then *if* there

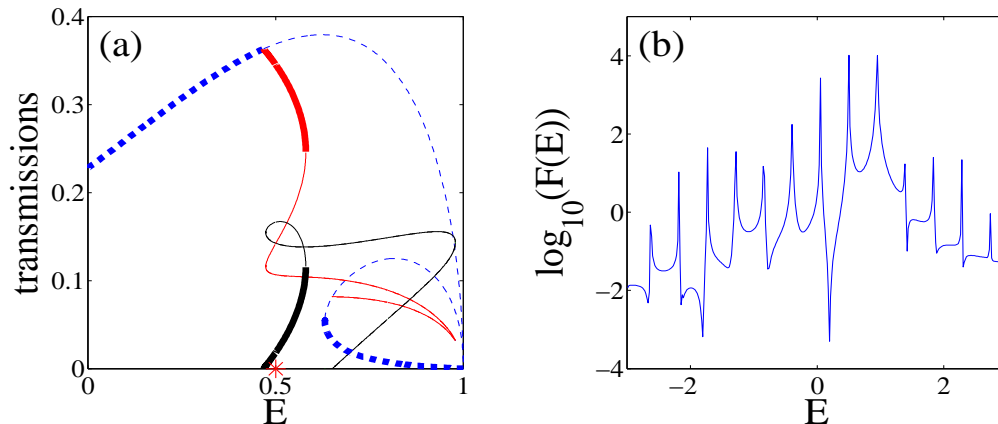


FIG. 9: (Color online) (a) Response of nonlinear plaquette to symmetric probing wave $\epsilon = 0.4, \gamma = 1, \lambda = 0.4, A_0 = 1$. Transmission probability $|T_{11}|^2$ for symmetry preserving solutions - dashed blue line, $|T_{11}|^2$ SB solutions - solid red line, $|T_{12}|^2$ SB solutions - solid black. (b) Corresponding Fourier power spectrum of amplitude u_3 at $E = 0.5$ (red star in Fig. 9(a)).

are stationary solutions (4) the standard procedure of matching reflected/transmitted waves (5) can be applied to obtain the transmission/reflection coefficients. It is more convenient, however, to use the Feshbach projection technique to project the total Hilbert space onto the space of the inner states that describe the scattering region only [26–28, 30]. The resulting equation could be seen as a nonlinear equivalent of the Lippmann-Schwinger equation (6) where H_{eff} is the nonlinear non hermitian effective Hamiltonian whose matrix elements depend in turn on the amplitude of the injected wave. The corresponding equations are written down for both dimer by Eq. (7) and and four-site square nonlinear plaquette Eq. (10). The effective Hamiltonian differs from the nonlinear Hamiltonian considered in Refs. [2–7, 10] due to the presence of dissipative terms $\epsilon^2 \exp(ik_p)$ where ϵ is the hopping matrix element that controls the coupling between the closed system and the waveguides.

In case of transmission of a symmetric plane wave through the nonlinear dimer we found two families of solutions. In the symmetry preserving family the incident symmetric wave is reflected and transmitted into the same symmetric channel. The second family, however, violates the symmetry of the probing wave. It means that when a symmetric wave is injected into the system the SB gives rise to emission of the antisymmetric plane waves and vice versa. Therefore the nonlinear dimer is capable for the mode conversion, although, with maximum efficiency around 50%. We found that the direct solution of the time-dependent Schrödinger equation with a wave front incident to the nonlinear dimer gives the same results for the transmission probabilities as found from the approach of the non-Hermitian Hamiltonian. It should be pointed out that the key feature that makes possible to access the SB solutions is the presence of domains in the parameter space where all symmetry preserving solutions are unstable. It means that in course of time the symmetry preserving solution will eventually collapse due to the presence of noise. The second important aspect about the open nonlinear dimer is that symmetry is broken by both intensity and phase of the scattering function.

Similar consideration was made for the open nonlinear four-site plaquette (see Fig. 1 (b)). Its closed counterpart has the symmetry group D_4 that provides many opportunities for the symmetry breaking [10]. However the presence of the waveguides in the design shown in Fig. 1 (b) substantially reduces this symmetry to the symmetry of the open dimer. Therefore one can expect a similar scenario for SB. However, in the case of plaquette four nonlinear degrees of freedom participate in the transmission which dramatically changes the dynamical picture. The standard theory of stability [43, 44] based on small perturbation technique reveals that there are domains in the parameter space where *none* of the stationary solutions (neither symmetry preserving nor symmetry breaking) are stable. It means that the scattering problem could not be reduced to stationary equations. Direct solution of the time-dependent Schrödinger equation revealed the emission of satellite waves at the energies different from the energy of incident wave provided that this energy is chosen within the domain where the symmetry preserving solution is unstable. The number of satellite wave and their energies depend mostly on the intensity of injected wave (or equivalently on the nonlinearity constant). This effect is different from the second harmonic generation with satellite energies not equal twice the injected wave energy. Emergence of additional equidistant peaks in the Fourier power spectrum of four-site nonlinear system was reported almost 30 years ago in the seminal paper by Eilbeck *et al* [2]. We believe that nowadays with the ongoing development of experimental techniques, in particular in handling photonic crystal waveguides, that phenomenon opens a new opportunity for harmonics generation. Another interesting possibility for constructing nonlinear quantum double-chain set-ups could be Bose-Hubbard ladders in optical lattices [49].

Acknowledgments

The work was supported by Integration grant N29 from Siberian Branch of RAS and RFBR grant N13-02-00497. The paper benefited from discussions with A.S. Aleksandrovsky, A.R. Kolovsky, E.N. Bulgakov, K.N. Pichugin, and M.Yu. Uleysky.

-
- [1] N.N. Akhmediev, Sov. Phys. JETP, **56**, 299 (1982).
 - [2] J.C. Eilbeck, P.S. Lomdahl, and A.C. Scott, Physica **16D**, 318 (1985).
 - [3] G.P. Tsironis and V.M. Kenkre, Phys. Lett. A **127**, 209 (1988).
 - [4] V.M. Kenkre and H.-L. Wu, Phys. Lett. A **135**, 120 (1989).
 - [5] V.M. Kenkre and M. Kuś, Phys. Rev. **B49**, 5956 (1994).
 - [6] L.J. Bernstein, Physica **D53**, 240 (1991).
 - [7] G.P. Tsironis, W.D. Deering and M.I. Molina, Physica **D68**, 135 (1993).
 - [8] M.I. Molina, Mod. Phys. Lett. **13**, 225 (1999).
 - [9] V.A. Brazhnyi and B.A. Malomed, Phys. Rev. **A83**, 053844 (2011).
 - [10] C. Wang, G. Theocharis, P.G. Kevrekidis, N. Whitaker, K.J.H. Law, D.J. Frantzeskakis, and B.A. Malomed, Phys. Rev. **E80**, 046611 (2009).
 - [11] K. J. H. Law, L. Qiao, P.G. Kevrekidis, and I.G. Kevrekidis, Phys. Rev. **A77**, 053612 (2008).
 - [12] T. Yabuzaki, T. Okamoto, M. Kitano, and T. Ogawa, Phys. Rev. **A29**, 1964 (1984).
 - [13] K. Otsuka and K. Ikeda, Opt. Lett., **12**, 599 (1987).
 - [14] M. Haelterman and P. Mandel, Opt. Lett., **15**, 1412 (1990).
 - [15] I.V. Babushkin, Yu.A. Logvin, and N.A. Loiko, Quant. Electronics, **28**, 104 (1998).
 - [16] P.G. Kevrekidis, Zh. Chen, B.A. Malomed, D.J. Frantzeskakis, and M.I. Weinstein, Phys. Lett. **A340**, 275 (2005).
 - [17] B. Maes, M. Soljačić, J.D. Joannopoulos, P. Bienstman, R. Baets, S.-P. Gorza, and M. Haelterman, Opt. Express, **14**, 10678 (2006).
 - [18] S. Shwartz, R. Weil, M. Segev, E. Lakin, E. Zolotoyabko, V.M. Menon, S.R. Forrest, and U. El-Hanany, Opt. Express, **14**, 9385 (2006).
 - [19] K. Aydin, I.M. Pryce, and H.A. Atwater, Opt. Express, **18**, 13407 (2010).
 - [20] Rujiang Li, Fei Lv, Lu Li, and Zhiyong Xu, Phys. Rev. A **84**, 033850 (2011).
 - [21] E.N. Bulgakov, K.N. Pichugin, and A.F. Sadreev, Phys. Rev. B **83**, 045109 (2011).
 - [22] E. Bulgakov and A. Sadreev, Phys. Rev. B **84**, 155304 (2011).
 - [23] S. Lepri and B.A. Malomed, Phys. Rev. **E87**, 042903 (2013)
 - [24] B. Maes, M. Fiers, and P. Bienstman, Phys. Rev. **A80**, 033805 (2009).
 - [25] E.N. Bulgakov and A.F. Sadreev, J. Opt. Soc. Am. **B29**, 2924 (2012).
 - [26] H. Feshbach, Ann. Phys. (NY) **5**, 357 (1958); *ibid* **19**, 287 (1962).
 - [27] I. Rotter, Rep. Prog. Phys. **54**, 635 (1991).
 - [28] S. Datta, *Electronic transport in mesoscopic systems*, Cambridge University Press (1995).
 - [29] F.-M. Dittes, Phys. Rep. **339**, 215 (2000).
 - [30] A.F. Sadreev and I. Rotter, J. Phys. A: Math. Gen. **36**, 11413 (2003).
 - [31] H.A. Haus, *Waves and Fields in Optoelectronics* (Prentice-Hall, N.Y., 1984).
 - [32] C. Manolatou, M. J. Khan, S. Fan, P. R. Villeneuve, H. A. Haus, and J. D. Joannopoulos, IEEE J. Quantum Electron. **35**, 1322 (1999).
 - [33] S. Fan, W. Suh, and J.D. Joannopoulos, J. Opt. Soc. Am. **A20**, 569 (2003).
 - [34] W. Suh, Z. Wang, and S. Fan, IEEE J. of Quantum Electronics, **40**, 1511 (2004).
 - [35] A.R. McGurn, Chaos, **13**, 754 (2003); J. Phys.: Condens. Matter **16**, S5243 (2004).
 - [36] A.E. Miroshnichenko, S.F. Mingaleev, S. Flach, and Yu.S. Kivshar, Phys. Rev. **E71**, 036626 (2005).
 - [37] S. Longhi, Phys. Rev. **B75**, 184306 (2007).
 - [38] A.E. Miroshnichenko and Yu.S. Kivshar, Phys. Rev. **E72**, 056611 (2005).
 - [39] S.F. Mingaleev, A.E. Miroshnichenko, Yu.S. Kivshar, and K. Busch, Phys. Rev. E **74**, 046603 (2006).
 - [40] A.E. Miroshnichenko, Yu. Kivshar, C. Etrich, T. Pertsch, R. Iliew, and F. Lederer, Phys. Rev. **A79**, 013809 (2009).
 - [41] A.E. Miroshnichenko, Phys. Rev. **E79**, 026611 (2009).
 - [42] M.F. Yanik, S. Fan, and M. Soljačić, Appl. Phys. Lett. **83**, 2739 (2003).
 - [43] N.M. Litchinitser, C.J. McKinstrie, C.M. de Sterke, and G.P. Agrawal, J. Opt. Soc. Am. **B18**, 45 (2001).
 - [44] A.R. Cowan and J.F. Young, Phys. Rev. **E68**, 046606 (2003).
 - [45] J. Joannopoulos, S.G. Johnson, J.N. Winn and R.D. Meade, *Photonic Crystals: molding the flow of light* (Princeton University Press, Princeton, N Y, 2008)
 - [46] C. Besse, SIAM J. Numer. Anal. **42**, 934 (2004).
 - [47] A. F. Oskooi, L. Zhang, Y. Avniel, S.G. Johnson, Opt. Express **16**, 11377 (2008).
 - [48] G.H.C. New and J.F. Ward, Phys. Rev. Lett. **19**, 556 (1967).
 - [49] A. Dhar, M. Maji, T. Mishra, R.V. Pai, S. Mukerjee, A. Paramekanti, Phys. Rev. A **85**, 041602(R)(2012).